Japan/USA Symposium on Flexible Automation
Volume 2
ASME 1996

PHYSICALLY-ACCURATE SYNTHETIC IMAGES FOR MACHINE VISION DESIGN

Johne' M. Parker and Kok-Meng Lee
George W. Woodruff School of Mechanical Engineering
Georgia Institute of Technology
Atlanta, Georgia 30332-0405

Abstract

In machine vision applications, accuracy of the image far outweighs image appearance. This paper presents physically-accurate image synthesis as a flexible, practical tool for examining a large number of hardware/software configuration combinations for a wide range of parts. Synthetic images can efficiently be used to study the effects of vision system design parameters on image accuracy, providing insight into the accuracy and efficiency of image-processing algorithms in determining part location and orientation for specific applications, as well as reducing the number of hardware prototype configurations to be built and evaluated.

We present results illustrating that physically accurate, rather than photo-realistic, synthesis methods are necessary to sufficiently simulate captured image gray-scale values. The usefulness of physically-accurate synthetic images in evaluating the effect of conditions in the manufacturing environment on captured images is also investigated. The prevalent factor investigated in this study is the effect of illumination: the significance of ambient lighting effects on the captured image and, therefore, on camera calibration was shown; if not fully understood, these effects can introduce apparent error in calibration results. While synthetic images cannot fully compensate for the real environment, they can be efficiently used to study the effects of ambient lighting and other important parameters, such as true part and environment reflectance, on image accuracy. We conclude with an evaluation of results and recommendations for improving the accuracy of the synthesis methodology.

1. INTRODUCTION

For machine vision system applications such as part presentation, the accuracy of image gray-scale pixel values far outweighs image appearance [Lee, 1991]; in this paper, we present physically-accurate image synthesis as a rational basis for designing both hardware and software components of a vision system. This is a very complex task, since such systems consist of many parts and the most proficient systems are designed by considering the *integrated* hardware/software arrangement. Numerical simulation is a flexible, practical tool for investigating a large number of hardware/software configuration combinations for a wide range of parts.

Prior machine vision research includes the use of *photo-realistic* synthetic images as an aid in testing model-based vision algorithms [Wu *et al*, 1990]; however, these images were generated with the simple image synthesis algorithms available with most commercial CAD systems, which assumed idealized or nonphysical reflectance models, limited light source models and unrealistic camera optics. While the images obtained with these packages were useful in gaining some insight into algorithm performance, their usefulness was limited [Chen and Mulgaonkar, 1991]. These photo-realistic images were generated based upon work developed in the area of computer graphics, where appearance of the image to the viewer is generally the primary concern. Meyer *et al* [1986] modeled the generation of a physically-accurate synthetic image. In their model, the environment description includes the scene's reflective and emitting properties, in addition to geometrical information and is processed via a simulation based upon the *physics* of illumination, instead of the idealized or nonphysical reflectance and illumination models used to produce photo-realistic images.

It was, in fact, attempts to improve the realism of photo-realistic images that resulted in the development of highly accurate methods for calculating illumination, which supported the development of *physically-accurate* synthesis methods [Goral et al, 1984; Nishita and Nakamae, 1985; Sillion *et al*, 1991, Kajiya, 1986; Ward *et al*, 1988]. The use of such physically-accurate images in an iterative method for improved image understanding was proposed by Gagalowicz [1990]. Some researchers, while agreeing that understanding the illumination problem is important, felt that most physically-accurate synthesis methods were too computationally expensive to be useful in vision system design [Cowan, 1991]. Rushmeier *et al* [1992] have developed an efficient methodology for generating physically-accurate synthetic images that predict the gray-scale values of images captured by a computer vision system. Results from this research confirm that physically-accurate image synthesis methods, rather than those methods currently available with standard CAD packages, are

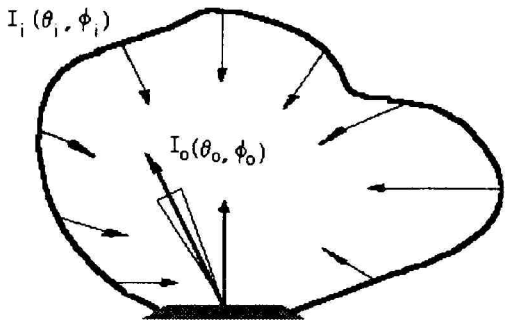

Figure 2. Model of radiance leaving a surface

The incident radiance, $I_i(\theta_{v,i}, \phi_{v,i})$, may originate at light sources or be due to multiple interreflections within the environment. A light source visible in direction $(\theta_{v,i}, \phi_{v,i})$ contributes an incident radiance equivalent to the emitted radiance of the source in that direction. If something other than a light source is visible in direction $(\theta_{v,i}, \phi_{v,i})$, this equation is recursive and its complete solution accounts for all possible geometric illumination effects, e.g., shadowing, highlights, etc.

The non-linearity of the gray-scale response of an imaging sensor is specified by an exponent "gamma λ" and thus, the sensor for a computer vision system is modeled here as a power law [Lee, 1994] as follows:

$$G_{pixel} = K\left(\int_0^\infty E_{pixel}(\lambda)s(\lambda)d\lambda\right)^\gamma + G_o \qquad (5)$$

where

G_{pixel} = pixel gray-scale value,
G_o = dark-current (zero illumination) value, and
$E_{pixel}(\lambda)$ = pixel energy/area value.

Equations (2)-(5) provide an analytical model for generating the output signal for a computer vision system characterized by sensor sensitivity K and system response linearity γ . K and γ are empirically-determined constants and $s(\lambda)$ characterizes the sensor as a function of wavelength for a given sensor. A gamma of unity yields a linear response, whereas less than unity compresses the bright end and greater than unity compresses the dark end. In Equation (5), the average energy incident over the pixel area is calculated from Equations (2) and (3), which require the solution to Equation (4).

At this point, it is worthwhile to point out the primary differences between the photo-realistic and physically-accurate image generation processes, using the governing equations given above: Photo-realistic images are usually generated using limited light source (e.g., parallel or isotropic point light sources) and optics (i.e., infinitesimal pinhole) models, idealized or nonphysical (i.e., Lambertian or Phong) reflectance models, and spectral dependence is usually ignored. Physically-accurate synthesis methods, on the other hand, are able to incorporate finite aperture and lens effects [Equation (3)], include spectral dependence [Equation (2)] and sensor non-linearity [Equation (5)], as well as model reflectance properties (e.g., specular, diffuse, anisotropic) and illumination distributions realistically [Equation (4)].

3. PHYSICALLY-ACCURATE IMAGE SYNTHESIS

Figure 3 compares the processes used to generate synthetic images for (a) photo-realistic and (b) physically-accurate synthetic images for vision system applications. As shown in Figure 3, an accurate mathematical model is needed to describe the physical scene and the vision system used to capture that scene. This model is used to simulate scene illumination, which is represented as an array of [pixel] radiances. This array of radiances is then converted to energy/area values, which are transformed by a mapping based on a model of the system sensor and how it converts incident light energy into gray-scale values.

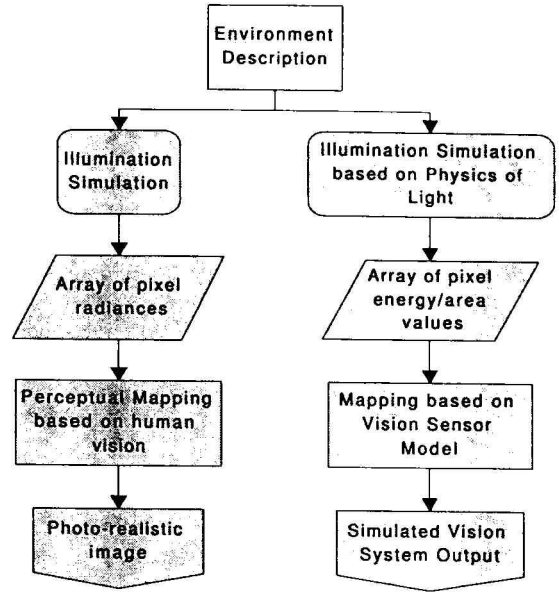

(a) Photo-realistic (b) Physically-accurate

Figure 3. Model of the synthetic imaging process

The physically-accurate synthetic image is simulated in a two step process. In the first step, *RADIANCE*, a freely-distributed software package from the Lighting Systems Research Group of the Lawrence Berkeley Laboratory, is used to solve the radiative heat transfer equation, Equation (4). In the second step, the sensor model for the computer vision system is modeled using the power law given in Equation (5).

The specific Monte Carlo solution method used in *RADIANCE* has been validated by both physical measurements and comparison with other software packages written to calculate illumination [Grynberg, 1989]. However, both the sensor pixels and pinhole, though small, have finite size that can not be accurately approximated by the infinitesimally small pixels and pinhole assumed by *RADIANCE*. This problem can be separated into two parts, and each solved separately. The first problem, that of finite pixel size, is minimized in *RADIANCE* by assuming an infinitesimal pinhole, shooting many rays through each pixel (i.e. sampling over the pixel area) and averaging the radiance values calculated for each ray. *RADIANCE* software does not have an explicit mechanism for

The effects of ambient illumination are illustrated in the following captured images and image histograms (Figure 7). The (wood) background is indiscernible from the board background for the controlled lighting case (in which ambient lighting was blocked with two layers of black felt); however, it can be seen for the ambient lighting case, showing the influence of additional illumination on the captured images. Note that the image histograms also clearly reflect this difference.

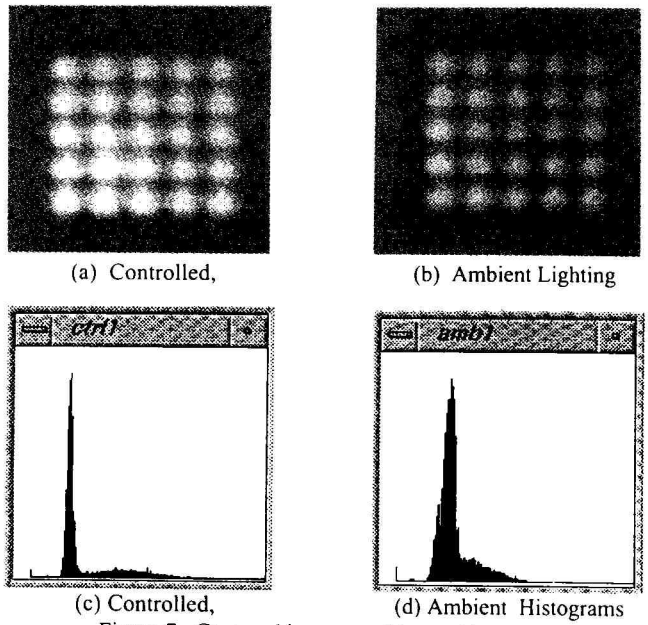

(a) Controlled, (b) Ambient Lighting

(c) Controlled, (d) Ambient Histograms

Figure 7. Captured images and image histograms

The effect of ambient illumination on camera calibration was shown by performing a camera calibration in ambient lighting and then using that information to determine the image accuracy for both ambient and controlled lighting conditions. Twenty images were captured for both lighting configurations; the centroids of the 25 retroreflective dots in each image were then calculated using image gray-scale values. The average vertical center-to-center distances for both the ambient and controlled lighting cases are given in Table 1.

Table 1. Effect of lighting conditions on average calculated center-to-center distances.

Lighting Condition	Average Distance	Standard Deviation
Ambient	19.052 mm	0.199 mm
Controlled	19.196 mm	0.215 mm

As expected, the average distance for the ambient case is essentially equivalent to the board center-to-center distance; additionally, the standard deviation concurs with the average RMS error reported by the FIVS calibration (x-error = 0.262, y-error = 0.274). The slightly high average distance reported by the images captured in controlled lighting illustrates the influence of ambient illumination on the image accuracy and, therefore, camera calibration.

Determination of Vision System Parameters

To determine the values of K and γ for the system, a single AiGaAs LED (with a 7° cone angle) was chosen as the illumination source and positioned as shown in Figure 4. Subsequent captured images represented a wide range of exposure times, ensuring that a full range of experimental gray-scale output values (from the dark current value to saturation) was obtained. The dark current gray-scale value was 22 and the saturation value, G_{max}, was 181. The values of K and γ were determined using the method of least squares, yielding a K value of 3.38×10^4 and a γ of 0.85.

Synthetic images of the retroreflective background were generated and compared to a captured image of the retroreflective field (Figure 8). As seen in Figure 9(a), a CAD-generated image assuming an ideal diffuse surface results in an image which is nearly black. Figure 9(b) illustrates *RADIANCE's* ability to model the retroreflective background; however, the illuminated area is too small and too sharply defined. Incorporation of the finite aperture (Figure 9(d)) results in an image with a more acceptable transition between the illuminated and non-illuminated areas, but the illuminated area is still too small. The importance of accurate source emission distribution modeling is shown in Figure 9(c).

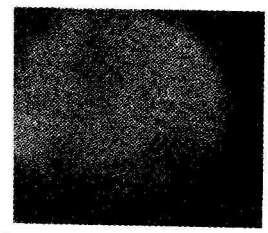

Figure 8. Captured Image of Retroreflective Field

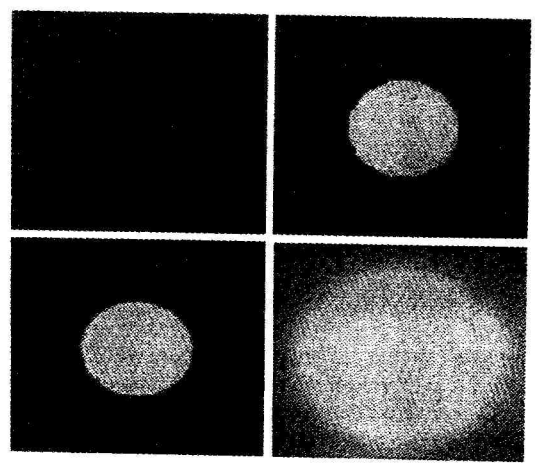

Figure 9. Synthetic images of Retroreflective field — Clockwise from upper-left-hand corner: a) generated with a CAD-package reflectance model, b) *RADIANCE*-generated image, using infinitesimal pinhole and cone-angle illumination model, c) image with finite pinhole model and Gaussian illumination distribution, d) finite pinhole, cone-angle illumination model.

Sobel operator to perform poorly. [A factor is determined to be significant if the absolute value of its t-value is greater than $t_{.025,16} = 2.12$] Note that part reflectance was *not* significant in determining algorithm performance, further substantiating the use of retroreflective materials to facilitate reliable image capture.

5. CONCLUSIONS

This paper discusses a method for generating physically accurate synthetic images for manufacturing applications where accurate location and orientation of the object outweigh its appearance. The synthesis method is able to incorporate finite aperture and lens effects, includes spectral dependence and sensor non-linearity, as well as models reflectance properties (e.g., specular, diffuse, anisotropic) and illumination distributions realistically.

The physically-accurate synthetic image is simulated in a two step process. In the first step, *RADIANCE*, a freely-distributed software package from the Lighting Systems Research Group of the Lawrence Berkeley Laboratory, is used to solve the radiative heat transfer equation. In the second step, differences between photo-realistic and physically-accurate images are highlighted, and methods to overcome limitations for generating physically accurate images are discussed: Physically-accurate pixel values are related to the energy/area falling on the sensor pixel and must be transformed by a mapping based on the vision sensor model. Modeling the relationship between pixel gray-scale and energy/area values as a power law, and using the empirically-determined sensitivity constants for the FIVS system results in synthetic images which more correctly predict captured image values. Furthermore, the results show that both the sensor pixels and pinhole, though small, have finite size that can not be accurately approximated by infinitesimally small pixels and pinholes; as demonstrated, the finite pinhole sampling method produces significantly improved images. Additionally, the significance of ambient lighting effects on the captured image and, therefore, on the camera calibration was shown; if misunderstood, these effects can introduce apparent error in calibration results, which include the focal length, lens distortion and the transformation to determine part location and orientation. While synthetic images cannot fully compensate for the real environment, they can be efficiently used to study the effects of ambient lighting and other important parameters, such as true part and environment reflectance, geometric alignment, etc. on image accuracy.

Future work includes investigating improved reflectance and illumination modeling; this provides significant opportunities for improvement: It is unlikely that the simple reflectance modeling used to represent the board background or the retroreflective dots is sufficient to adequately predict captured-image performance. Also, the light sources chosen for the FIVS system are unlikely to be identical and may vary significantly from the typical pattern used in the simulations shown above (e.g., the distribution pattern may not be symmetrical). Distribution of ambient lighting sources may vary similarly. After addressing these issues and sufficiently validating the methodology, simulated images will be used to study a variety of hardware design parameters and their effects on image accuracy.

ACKNOWLEDGEMENTS

This work is partially supported by the NSF Graduate Fellowship and the Woodruff Faculty Fellow Award.

REFERENCES

Chen, C.-H. and Mulgaonkar, P. G., 1991, "CAD-Based Feature Utility Measures for Automatic Vision Programming," IEEE Workshop on Directions in Automated CAD-Based Vision, Maui Hawaii, IEEE Computer Society Press.

Cowan, C., 1991, "Automatic Camera and Light-Source Placement Using CAD Models," IEEE Workshop on Design in Automatic CAD-Based Vision, Maui Hawaii, IEEE Computer Society Press.

Gagalowicz, A., 1990, "Collaboration Between Computer Graphics and Computer Vision," in Scientific Visualization and Graphic Simulation, ed. by D. Thalmann, pp. 233-248.

Goral, C. M., Torrance, K. E., Greenberg, D. P. and Battaile, B., 1984, "Modeling the Interaction of Light Between Diffuse Surfaces," Computer Graphics, V. 18, N. 3, pp. 213-222.

Grynberg, A., 1989, "Validation of Radiance," Lawrence Berkeley Laboratory, Applied Sciences Division, Lighting Systems Research Group, Report #LBID 1575.

Kajiya, J. T., 1986, "The Rendering Equation," Computer Graphics, V. 20, N. 4, pp. 143-150.

Lee, K.-M., 1991, "Flexible Part-Feeding System for Machine Loading and Assembly, Part I - A State-of-the-Art Survey," "Part II- A Cost Effective Solution," International Journal of Production Economics, V. 25, pp. 141-168.

Lee, K. M., 1994, "Design Concept of an Integrated Vision System for Cost-Effective Part Presentation," ASME Transactions on Engineering in Industry, V. 116, pp. 421-428.

Lee, K.-M. and Blenis, R., 1994, "Design Concept and Prototype Development of a Flexible Integrated Vision System," Journal of Robotic Systems, Vol. 11, No. 5, pp. 387-398.

Meyer, G. W., Rushmeier, H. E., Cohen, M. F., Greenberg, D. P. and Torrance, K. E., 1986, "An Experimental Evaluation of Computer Graphics Imagery," ACM Transactions on Graphics, V. 5, N. 1, pp. 30-50.

Nishita, T. and Nakamae, E., 1985, "Continuous Tone Representation of Three Dimensional Objects Taking Account of Shadows and Interreflections," Computer Graphics, V. 19, N.4 pp. 23-30.

Rennilson, J. J., 1980, "Retroreflective Measurements" A Review," Applied Optics, Vol. 19, No. 8.

Rushmeier, H. E., Parker, J. M. and Lee, K. M., 1992, "Synthetic Images for Cost-Effective Machine Vision / Illumination Design," SME Applied Machine Vision Conference Proceedings.

Siegel, R. and Howell, J. R., 1981, *Thermal Radiation Heat Transfer*, Hemisphere, Washington, DC.

Sillion, F. X., Arvo, J. R., Westin, S. H. and Greenberg, D. P., 1991, "A Global Illumination for General Reflectance Distributions," Computer Graphics, V. 25, N. 4, pp. 187-198.

Tsai, R. Y., 1987, "A Versatile Camera Calibration Technique for High Accuracy 3-D Machine Vision Metrology Using Off-the-Shelf TV Camera and Lenses," IEEE Robotics and Automation, Vol. RA-3, N. 4, pp. 323-344.

Ward, G. J., Rubinstein, F. M. and Clear, R. D., 1988, "A Ray Tracing Solution for Diffuse Interreflections" Computer Graphics, V. 22, N. 4, pp. 85-92.

Wu, C. K., Cheatham, J. B., Lin, Y. H. and Cleghorn, T. F., 1990, "Computer Graphics Modelling for Simulating and Testing Robot Vision Systems," International Journal of Modelling and Simulation, V10, pp. 67-70.

necessary to sufficiently simulate captured images. Highly-accurate methods of calculating illumination establish the basis for generating the array of pixel radiances representing scene illumination. Most graphics methods, however, assume an infinitesimal pinhole to find a solution for the rendering equation [Kajiya, 1986], which calculates the average radiance incident on each image pixel for a wavelength band.

The benefits of this research are three-fold: First, it provides a rational basis for designing the hardware and software components of a machine vision system. Secondly, this research introduces a methodology for comparing algorithms and predicting the optimal algorithm (and optimal performance) for a specific application. Additionally, it provides an opportunity to perform an in-depth study of the factors that can significantly degrade the performance of image-processing algorithms and aid in the determination of critical design parameters. A third contribution is the ultimate development of a well-designed CAD-tool which utilizes physically-accurate synthetic images to accurately and inexpensively predict the performance of a proposed vision system design prior to implementation or the construction of a prototype, minimizing the need to build and test a large number of hardware configurations. Such a tool also allows necessary changes in part design to be made earlier in the design phase, significantly reducing implementation time and improving industrial reliability.

The remainder of this paper is organized as follows: the theory of physically-accurate synthetic image generation, which includes a discussion of the governing equations necessary to generate physically-accurate images is followed by a detailed comparison of the differences between photo-realistic and physically-accurate synthesis methods. The Experimental Investigation section begins with a description of the hardware testbed, followed by a discussion of the computational model for radiative transfer, which provides the foundation for physically-accurate image synthesis. This is followed by the results of the specific experiments performed to better understand the effect of parameters, especially [source and ambient] illumination; the paper concludes with a discussion of the results and recommendations for future work.

2. FUNDAMENTAL EQUATIONS

The geometry of the illumination incident at each image pixel is diagrammed in two dimensions in Figure 1. Radiance incident on the sensor pixel is equal to the radiance leaving the real-world object that is visible to the sensor through the pinhole. The solid angle of the cone rays leading to the patch on the object is equal to that corresponding patch in the image. Thus, it can be shown that the irradiance (or the power per unit area) incident on the surface of a pixel is given by

$$I_i(\theta_{p,i}, \phi_{p,i}) = I_o(\theta_{p,i}, \phi_{p,i}) \cos\theta_{p,i}\, d\omega \qquad (1)$$

where

θ, ϕ = spherical coordinates (θ is the polar angle and ϕ, the azimuthal angle) specifying the direction in three dimensional space,

$I_i(\theta_{p,i}, \phi_{p,i})$ = irradiance falling on a point (x_p, y_p) on the pixel along the ray from the object, and

$I_o(\theta_{p,i}, \phi_{p,i})$ = radiance (or the power per unit area per unit solid angle) from the object in the direction toward the pinhole.

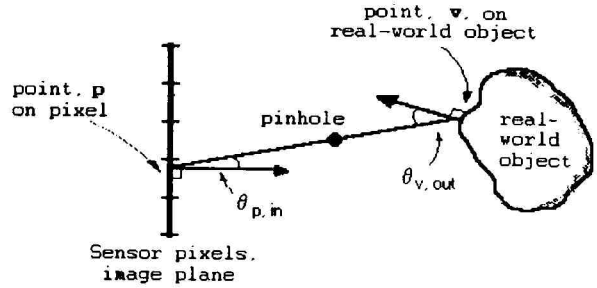

Figure 1. Geometry of illumination simulation for an infinitesimal pinhole camera.

In machine vision, captured image values are proportional to $E_{pixel}(\lambda)$, the average *energy/area* incident on the sensor pixel, or

$$E_{pixel}(\lambda) = \int_{pixel-area} E_i(\theta_{p,i}, \phi_{p,i}) f(x_p, y_p, \lambda)\, dA_{pixel} \qquad (2)$$

where $E_i(\theta_{p,i}, \phi_{p,i})$ is the energy/area incident on the sensor pixel at that point along that direction and $f(x_p, y_p, \lambda)$ is the spatial sensor sensitivity for a given wavelength band at that point on the pixel. The energy/area incident on the pixel for a specified period of time τ can be solved by integrating the irradiance over the pinhole area as follows

$$E_i(\theta_{p,i}, \phi_{p,i}) = \int_{pinhole} I_o(\theta_{p,i}, \phi_{p,i}) \cos\theta_{p,i} \tau\, d\omega_{pinhole} \qquad (3)$$

where τ represents exposure time to scene illumination and ω is the solid angle subtended by the pinhole. The irradiance, $I_i(\theta_{p,i}, \phi_{p,i})$ is equal to that leaving the visible real-world object and depends on the irradiance falling on the surface from all directions. This irradiance may be from light sources or from secondary reflections from other surfaces in the environment. For reflective surfaces, the object radiance is not known a priori and must be calculated; its value depends on the light energy incident on the object (Figure 2) and is given by the equation of radiative transfer [Siegel and Howell, 1981]:

$$I_o(\theta_{v,o}, \phi_{v,o}) = \int_{\cap} \rho_{bd}(\theta_{v,o}, \phi_{v,o}; \theta_{v,i}, \phi_{v,i}) I_i(\theta_{v,i}, \phi_{v,i}) \cos\theta_{v,i}\, d\omega_i \qquad (4)$$

where

$\rho_{bd}(\theta_{v,o}, \phi_{v,o}; \theta_{v,i}, \phi_{v,i})$ = bi-directional reflectance of the object, and

$I_i(\theta_{v,i}, \phi_{v,i})$ = incident radiance on the real-world object at point (x_v, y_v) on the object, and the integral is over the entire hemisphere of directions above that object at that point.

integrating over a finite aperture; therefore, the array of radiances for the finite pinhole is found by taking the weighted average of radiances calculated for an infinitesimal pinhole at several different positions within the finite pinhole.

To transform the array of irradiances determined by the computational model into predicted gray-scale values corresponding to a particular system, K and γ, are calibrated experimentally for the *system* which accounts for the system non-linearity. Figure 4 suggests a general technique for calibrating K and γ, where a known illumination source of a single wavelength band is sampled. Therefore, the spectral sensitivity function $s(\lambda)$ is constant in Equation (5) and its contribution can be absorbed into the value for K. Note that the uncertainty in the value of the power output for the LED does not affect the value of γ; however, it would "scale" K, shifting the histogram of gray-scale values left or right. For a specified source of intensity S (power per unit solid angle) with an included angle of ε degrees, the small planar patch of area on the sensor at a distance D from the source subtends a solid angle of $\pi\tan^2(\varepsilon/2)$. Over an exposure time of τ seconds, the intensity of the source on the sensor is

$$E = S\pi\tan^2(\varepsilon/2)\tau. \quad (6)$$

A series of images can be obtained over a wide range of exposure times, ensuring that a full range of experimental gray-scale output values (from the dark current value to saturation)is obtained.

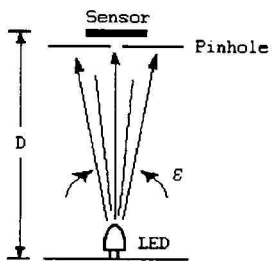

Figure 4 Calibration experimental setup

Figure 5 shows a schematic of the experimental setup where the imaging sensor, signal conditioning amplifier, and A/D converter are treated as an integrated unit. The relationship between the average gray scale value and the average energy of the source over the exposed area on the sensor can be determined from Equation (5), which can be rewritten in the following form to facilitate the determination of K and γ:

$$\ln(G-G_o) = \gamma \ln E + \ln K. \quad (7)$$

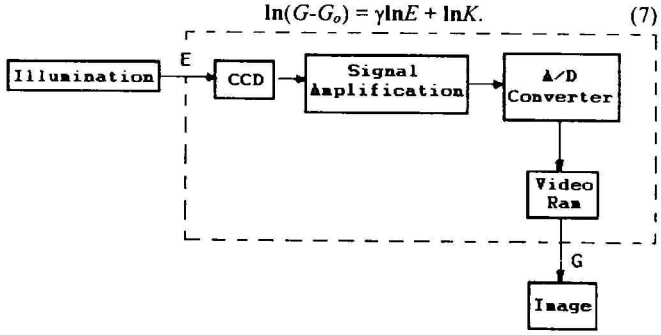

Figure 5. Calibration of System Response

4. EXPERIMENTAL INVESTIGATION

While the opportunity to increase image accuracy by studying and understanding the parameters which influence image accuracy exist in many areas, the most important parameters include illumination distribution and ambient lighting, part reflectance, and geometric alignment. This study concentrated on the effects of illumination distribution and ambient lighting on image accuracy and repeatability. Three experiments were conducted to examine the effects of design parameters on image accuracy: First, the effect of ambient lighting on captured images and thus on system accuracy was studied experimentally. Next, the sensor/system sensitivity and linearity (required in Equation 5) were empirically determined. Finally, experiments were conducted to study the sensitivity of a specific image-processing algorithm to four major design parameters using synthetic images (which were generated using the sensitivity constants determined in the second experiment).

The vision system chosen for this study is the FIVS (Flexible Integrated Vision System) developed at Georgia Tech [Lee and Blenis, 1994]. The configuration as shown in Figure 6 utilized a structured, co-located illumination system consisting of twelve AiGaAs LED's (with a 7° cone angle) placed circumferentially (in a 25 mm diameter) around the lens (focal length = 10.59 mm).

Figure 6. FIVS Illumination System

This system as shown in Fig. 6 is an effective prototype for the validation of the proposed methodology for several reasons: The use of retroreflective materials in this application enables the capture of reliable gray-scale images with a high object-to-background contrast without a detailed prior knowledge of object geometry and surface reflectance. Retroreflective vision sensing also facilitates the use of low-power, low cost light sources for part presentation. The chosen CCD sensor has a strong spectral response at the dominant wavelength provided by the illumination sources and is reasonably insensitive to the effects of ambient lighting.

Effect of Ambient Illumination

A calibration board containing a 5x5 grid of retroreflective dots was the subject of captured and simulated images. The dots are circular areas of 5/8 inch diameter, spaced by a 3/4 inch (19.05 mm) center-to-center distance. The dots are placed on a background of partially diffuse black tape. Tsai's [1987] camera calibration was the algorithm used to examine the effects of source and ambient illumination.

The effects of ambient illumination are illustrated in the

Synthetic images of a calibration board were generated and compared against captured images under both controlled and ambient lighting conditions; for this study, the board was positioned at an angle of 34° to the diffuse background. Sample images are shown in Figure 10. The limitations of infinitesimal pinhole modeling are shown in image (b); averaging over the finite aperture results in an image (c) that more nearly reflects the gray-scale values of the captured image. While the synthetic images illustrate that the correct reflectance distribution (i.e., the ability to model retroreflective materials), pinhole model and light source distribution are critical in accurately simulating captured images, it is clear that much work remains to be done.

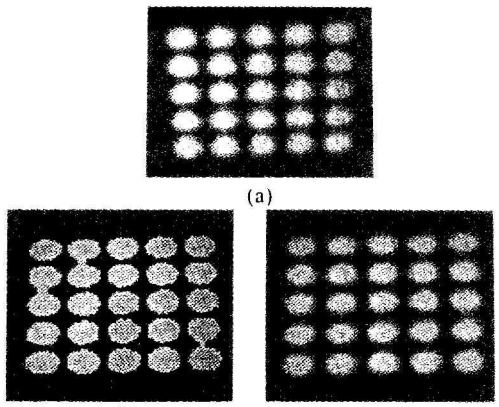

(a)

(b) (c)

Figure 10. (a) Actual Captured Image (b) Synthetic Image Assuming Infinitesimal Pinhole, (c) Physically Accurate Image with Finite Pinhole.

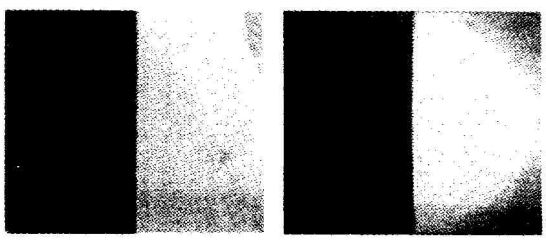

(a) Captured image (b) Synthetic Image

Figure 11. Edge Images

An experimental investigation of edge synthesis was also performed. A comparison of captured and synthetic images of the transition between a black diffuse surface and the retroreflective background is shown in Figure 11; an exploded view of the edge transition (Figure 12) shows the importance of the γ (sensor nonlinearity) calibration for the system. As seen in this figure, an edge model which doesn't account for sensor nonlinearity fails to predict the edge transition accurately. The actual edge shows a nonlinearity factor between 0.85 (the experimental value) and 0.90.

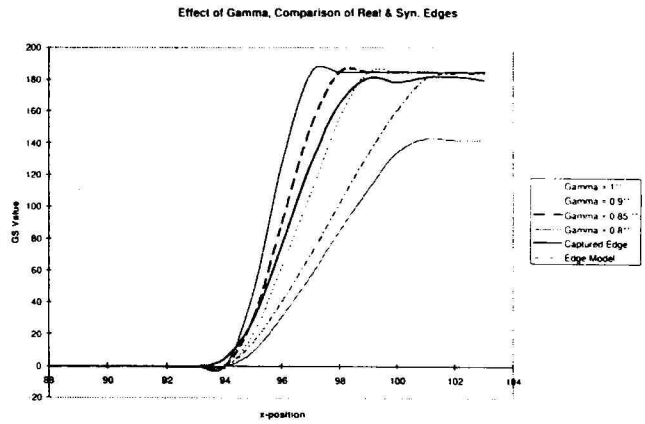

Figure 12. Effect of Gamma on Synthetic Edge Modeling

Factors Affecting Performance

The primary motivation of this investigation was to study the effects of four factors — camera angle, LED angle, part reflectance and part shape — on the performance of a specific image-processing algorithm. A 2^4 full factorial experiment was designed to generate the 16 synthetic images used to study the effects of the chosen factors on algorithm performance. The specific image-processing algorithm studied was the Sobel edge enhancement operator, which was used to enhance the edge locations of each synthetic image. Edges were extracted from each enhanced image using the same threshold value; this edge information was then used to determine the apparent length of the part. Table 2 summarizes the results. For each factor, two sets of eight samples corresponding to the high and low level are compared.

Table 2. Significance of the Four Design Parameters on Sobel Algorithm Performance

Factor Description	Low Level	High Level	t_i
A: Illumination angle (of LED's)	0°	5°	0.42
B: Camera (sensor/pinhole) angle	0°	10°	6.72
C: Reflectance of part	Diffuse	Specular	-0.13
D: Part Shape	Flat	Cylindrical	4.70

To eliminate the confounding of effects due to sensitivity to part location and size, both the cylindrical object (1 inch diameter and 1 inch length) and flat objects (1 inch by 1 inch square) were designed with the same projected area and location in the image. As a precaution, a ceiling was placed on part length, in case some edges were undetectable at the threshold value. Even prior to analysis, it was clear that camera angle (which affected field illumination) was significant— none of the images generated with a high level of factor B (a 10° camera angle) could correctly locate the part. Results of the study (Table 2) showed factors B and D (camera angle and part shape) and the interaction of BD to be significant in the performance of the Sobel operator; i.e., high levels of these factors caused the